PHYSICAL REVIEW B VOLUME 25, NUMBER 4 15 FEBRUARY 1982

Xerographic spectroscopy of gap states in amorphous semiconductors

M. Abkowitz and R. C. Enck
Xerox Corporation, 800 Phillips Road - 114, Webster, New York 14580
(Received 24 August 1981)

Analysis of the temperature-dependent decay of surface voltage on an amorphous film after charging but prior to exposure (xerographic dark decay) and of residual decay after exposure can, in combination, be used to map the density of states and position the Fermi level. The procedure is illustrated for *a*-Se where both electron and hole residuals can be measured. *a*-Se is found to be characterized by a relatively discrete gap-state structure. These measurements readily discern thermostructural and photostructural effects on gap-state populations. Thus, during structural relaxation of glassy films in the As:Se alloy system, systematic variation in a number of localized states distributed throughout the mobility gap is observed. This observation is consistent with the view that native defects play a key role in photoelectronic behavior of amorphous chalcogenides.

I. INTRODUCTION

Experimental techniques initially developed to characterize xerographic photoreceptors are widely applicable to the study of amorphous thin films. The xerographic measurements to be described monitor trapping during photoinjection and the subsequent thermally stimulated processes by which the charged semiconductor re-establishes space-charge equilibrium. It will be demonstrated that from such xerographic measurements information can be extracted about the nature and distribution of those electronic gap states which play a key role in influencing photoelectronic behavior.

In the sensitization-exposure part of the xerographic cycle[1] a photoreceptor film mounted on a grounded substrate is charged, typically by corona, then completely photodischarged by exposure to strongly absorbed light. For the photoreceptor structure to be useful in the xerographic mode both the top corona contact and the substrate contact should be blocking. The resulting capacitorlike structure contains a uniform field after charging in the dark. Illumination with strongly absorbed light creates a thin sheet of electron-hole pairs which separate under action of this field. Depending on charging polarity one sign of carrier acts to neutralize charge on the top surface while the opposite sign of carrier drifts through the bulk toward the grounded substrate. As a result of this carrier displacement the surface voltage decays in time (photoinduced discharge). The surface voltage would in fact decay to zero were it not for the fact that some fraction of the carriers in transit through the bulk became deeply trapped. The rapid photoinduced discharge terminates in a residual potential due to this trapped charge. Space-charge neutrality is reestablished on a longer time scale by thermally stimulated processes.

There is important information yielded at each stage of the xerographic cycle. For instance, by time resolving the charge delivered to an amorphous film from a corona or from transient contract to a power supply, one can discern injection phenomena and measure dielectric parameters. By measuring the temperature-dependent dark decay of surface voltage one can determine the spectral (energy) distribution of thermal generation centers.[2] By the latter technique or by measuring the dark discharge depletion time[3] (the time required for the bulk to generate some fixed quantity of charge under isothermal conditions) one can estimate the position of the Fermi energy. Analysis of photoinduced discharge can, depending on experimental conditions, be used to determine the parameters which characterize either photogeneration or transport.[4]

In the following, application of a new class of xerographic measurements based on analysis of residuals is emphasized. It will be shown that from analysis of residual buildup during repetitive cycling and from analysis of the isothermal decay of xerographic residual after cycling ceases, it is possible to map the spectral distribution of bulk traps in an amorphous film. The spatial distribu-

 ©1982 The American Physical Society

tion of trapped charge which gives rise to residual voltage can be determined in addition, by analyzing the pulse shape in a xerographic time-of-flight experiment (XTOF).[5] Xerographic measurements are extraordinarily sensitive in this application. In fact 10^{12} cm^{-3} uniformly trapped electrons can, in a typical sample film, give rise to several volts of surface potential which is easily measured. Initial application has been to chalcogenides.

In this paper a density-of-gap-states diagram is derived from xerographic measurements on amorphous Se. Amorphous Se is a particularly interesting chalcogenide (lone-pair semiconductor) prototype, because of its ambipolarity. The defect origin of deep traps and thermal-generation centers in *a*-Se is established by examining changes induced in xerographic residuals and in dark decay during structural relaxation.[6] It is demonstrated that equilibrium trap populations are fully established after 100 hours of annealing at room temperature independent of prior thermal history.[7] Finally it is demonstrated that prior bulk photoexcitation of *a*-Se enhances subsequent hole and electron deep trapping. This effect is metastable but decays away at different rates for electrons and holes.

The remainder of the paper is organized as follows: Section II discusses sample preparation and describes xerographic measurement apparatus and technique. The importance of experimentally determining the internal geometric distribution of the tapped space charge, which gives rise to residual, is emphasized. The results discussed in Sec. III are subdivided into five subsections. In Sec. III A the buildup of trapped space charge during xerographic cycling is discussed. The photoinjected carrier ranges can be calculated from the residual voltage developed on a well-rested film after a single cycle. The integrated number of traps (for either sign carrier) can be calculated from the saturation residual after repeated cycling only when certain conditions are satisfied. In Sec. III B analysis of positive and negative decay is described for *a*-Se. By combining these results with dark-decay data the position of the Fermi level is ascertained in Sec. III C. Xerographic data is combined with results of drift-mobility measurements (electrons and holes) to construct a composite density-of-states diagram for *a*-Se in Sec. III D. In Sec. III E the use of xerographic techniques to monitor thermostructural, light-induced, and chemically-induced mechanisms which effect changes in electron and hole deep trapping is described. Section IV summarizes key results.

II. EXPERIMENTAL

Samples investigated were films of *a*-Se. These were prepared by vacuum evaporation at a rate of 2 μm/min onto oxidized aluminum substrates held above the glass transition temperature. (Substrate temperature was typically 55 °C which is about 18 °C above the glass transition temperature.) The aluminum oxide layer which forms the substrate interface is approximately 50 Å thick. Film thicknesses ranged from 10 – 100 μm. Films prepared from a variety of source materials were compared.

Corona-mode xerographic measurements were carried out using a reciprocating sample stage. The sample stage was a large thermal mass in physical contact with a thermoelectric heater-cooler. In operation the sample is first passed under a corona-charging device, the corotron, which can be set to deposit either positive or negative ions on the sample surface. The charging circuitry is such that constant current can be supplied to the sample, simplifying the analysis of residual voltage cycle-up and xerographic time-of-flight data. After charging, the sample is moved to a measuring station where surface voltage is determined using a transparent, capacitively coupled electrometer probe. The time from termination of the charging step to the onset of surface voltage measurement is a few tenths of a second. Either the dark decay or the photoinduced-discharge characteristic (PIDC) following step or flash illumination with strongly absorbed light, can be measured. In addition the transit of a small packet of charge photoexcited at the top surface by a weak, 4 nsec pulse of strongly absorbed light could be time-resolved in the field established by prior corona charging. Small-signal time of flight could thus be measured for both carriers in the xerographic mode (XTOF).[5] XTOF can be used to both elucidate transport behavior and probe the internal-field distribution[8] (from which the space-charge distribution is determined) in the film at any time. After discharge, decay of residual potential can be time resolved. The entire sequence of charging, photodischarge, and residual can be continuously recycled. One consequence of cycling is the progressive, stepwise buildup of residual voltage.

Experimental diagnostics are required to establish the electrical nature of the top-surface (corona) contact and the substrate interface. In the present experiment both the corona contact and the oxidized aluminum substate contact are blocking for

both electrons and holes. The contacts are blocking in the conventional sense that they allow the sample structures to charge capacitively in the dark for both positive and negative corona. There is, in other words, no significant charge injection or sweep out observed during charging. For residual potential measurements it is the blocking nature of the substate contact which is of key importance (after complete photodischarge the top-surface field is zero). By blocking in this case we mean that the substrate injects substantially less than a CV_R (C is the sample capacitance and V_R the residual voltage immediately after photodischarge) of counter charge during the time required for the bulk-trapped space charge to release at a given temperature. An upper bound on the combined injection rate of top and substrate contacts is furnished by the dark decay (dark decay is the sum of injection and bulk thermal generation). In the samples studied here dark decay in fact proceeds much more slowly than residual decay. Substrate injection is therefore not significant on a practical time scale.

The exact structure of the substrate blocking contact is not known. We do not know, for instance, if interfacial chemistry and interdiffusion are significant. We do know that the thin Al_2O_3 substrate surface layer survives the film deposition process. A 50-Å Al_2O_3 layer would be incapable of sustaining voltages comparable to the residual voltages observed. It is nevertheless important to independently establish that the residual observed during xerographic cycling is due to bulk-trapped space charge and does not arise from charge buildup across an insulating interfacial layer. Very direct evidence bearing on this issue is furnished by XTOF experiments. XTOF experiments can quantitatively map the trapped space-charge distribution developing in a film specimen during xerographic cycling. The residual voltages observed in our samples are in fact completely accounted for by the bulk-trapped space charge.

Some xerographic measurements were carried out in the electroded mode. In this case sample films were supplied with semitransparent top contacts. Charging was by transient contact to a dc power supply with the entire sequence controlled by tandem pulse-delay generators or a microprocessor. Electroded xerographic measurements offer two advantages: (1) ability to vary the xerographic cycle parameters over an extremely wide range, and (2) ease in carrying out temperature dependence measurements over an extended range.

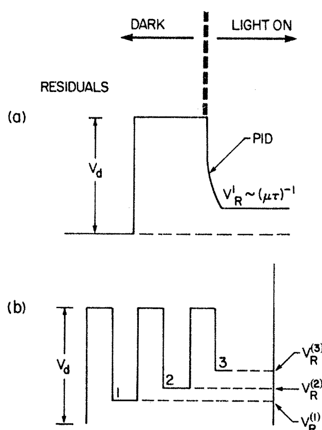

FIG. 1. (a) Schematic voltage profile of a sample during a single xerographic cycle. V_d is the voltage to which the sample is charged. After photoinduced discharge (PID) the residual potential is inversely proportional to the injected carrier $\mu\tau$ product. (b) Repeated xerographic cycling causes the residual to buildup ("cycle-up").

III. RESULTS

A. Cycle-up

Figure 1(a) shows the voltage profile of a sample during a single xerographic cycle. The cycle is initiated by a corona-charging step during which the sample film having capacitance C is charged to a voltage V_d of either polarity. During photodischarge (PID) by strongly absorbed light, some fraction of the transiting charge falls into deep traps and the resulting space charge is manifested as a residual potential V_R. With repeated cycling the residual builds up as shown in Fig. 1(b). The residual potential, measured using a capacitively coupled electrometer probe, can be related to the space-charge distribution function. Geometrical considerations reduce this to a one-dimensional formulation

$$V_R=\epsilon_0^{-1}\epsilon^{-1}\int_0^L dx\int_0^L \rho(x')dx' , \quad (1)$$

where L is the sample thickness, ϵ is the relative dielectric constant, ϵ_0 the free-space permitivity, and $\rho(x)$ the space-charge density. For the case of uniform bulk space charge of density ρ_0 the above simplifies:

$$V_R=\rho_0 L^2/2\epsilon_0\epsilon , \quad (2)$$

or equivalently,

$$V_R=NeL^2/2\epsilon_0\epsilon ,$$

when N is the number per unit volume of electronic charges e. Figure 2 illustrates that a relatively small density of surface or bulk-trapped charges on or in a typical xerographic film (i.e., $L=50$ μm) can give rise to an appreciable surface voltage. Figure 2, upper, is a plot of surface voltage versus surface density of electronic charges. Figure 2, lower, is a similar plot of surface voltage versus density of bulk-trapped charge computed using Eq. (2). Notice for example that as few as 10^{12} electronic charges per cm^3 in a 50-μm film ($\epsilon=6.4$) would give rise to a 4 V residual which is easily measured.

Consider next the effect on surface voltage of geometrical redistribution of a fixed number N of trapped charges in a given film. If for a uniform volume distribution of N charges the surface voltage is V_s it is $2V_s$ if the same N charges are all localized on the film's top surface. If the sample thickness is L, then for the case that trapped space charge is uniformly distributed in the top half of the sample volume (i.e., between the top surface and $L/2$) the surface voltage is $1.5V_s$. For the case of a uniform distribution of N charges in the lower half of the sample volume (i.e., from $L/2$ to L) the surface voltage is $0.5V_s$. For the case that the N charges are localized in the 10% of the sample volume immediately adjacent to the substrate the surface potential would be $0.1V_s$. Use of the spatially uniform trapping approximation to estimate the number of trapped charges from the residual potential thus introduces serious error only when the space-charge distribution is significantly skewed towards the substrate. Such extreme skewing is readily detected by the XTOF technique if the transients are nondispersive.[9] Monitoring of space-charge distributions in our samples using XTOF showed no extreme skewing and indicated that use of the uniform trapping approximation would introduce an error of less than a factor of 2 in the calculated trap density.

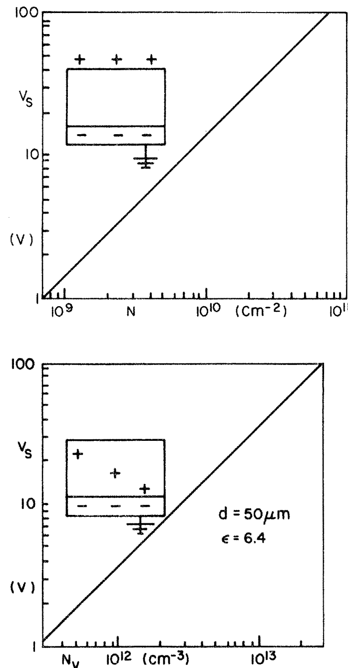

FIG. 2. Upper: surface voltage V_s vs surface density of electronic charges. Lower: surface voltage V_s versus volume density of electronic charges. Both computed for a 50 μm thick film, $\epsilon=6.4$.

The $\mu\tau$ product where μ is the drift mobility and τ the bulk deep trapping lifetime can be determined from the first-cycle residual potential of a well-rested sample of thickness L. In the weak trapping limit (the residual V_R is much less than the charging voltage V_d) Kanazawa and Batra[10] derive the expression

$$V_R/V_d=(0.5L^2/\mu\tau V_d)[-\ln(2V_R/V_d)] \ . \quad (3)$$

The above is to within a factor of 2, just the physically plausible expression derived by taking the residual to be that voltage for which the carrier range is nominally half the sample thickness[11]

$$V_R/V_d \simeq 0.5L^2/\mu\tau V_d \ . \quad (4)$$

In the strong trapping limit ($V_R \sim V_d$) Kanazawa and Batra derive[10]

$$V_R/V_d=1-(\mu\tau V_d/L^2)(\ln 2) \ , \quad (5)$$

which differs only slightly from the expression based on the above physical definition[11] of residual

$$V_R/V_d=1-(\mu V_d\tau/L^2) \ . \quad (6)$$

In general, bulk deep trapping lifetimes computed from first-cycle residuals are in agreement with lifetimes measured in the time-of-flight mode under range-limited conditions.[12] For example, in an a-Se specimen with $L=48$ μm charged to 200 V, hole and electron residuals at $T=295$ K were found to be 1.8 and 44 V, respectively. The measured drift mobilities, lifetimes, and $\mu\tau$ products for that specimen, for electrons and holes, respectively, are 4.9×10^{-3} cm^2/V sec, 5×10^{-5} sec, 2.45×10^{-7} cm^2/V, and 0.16 cm^2/V sec, 4.4×10^{-5} sec, 7.04×10^{-6} cm^2/V. The $\mu\tau$ product computed using Eq. (4) is 2.62×10^{-7} cm^2/V for electrons and 6.4×10^{-6} cm^2/V for holes.

Figure 3 illustrates the increase in positive resi-

dual potential with the number of xerographic cycles. There is a general tendency toward saturation on repeated cycling. For the sample illustrated, which is about 50 μm thick, the hole residual potential saturates after many hundred cycles at about 150 V. The sample was initially charged by corona to 750 V. The residual achieved was insensitive to the charging voltage when the latter was large compared to the residual voltage. Cycle time was 3 sec. Only limited experimental control of the xerographic cycle was possible in the corona apparatus used. Variation in the conditions of xerographic cycling were found to primarily affect the initial shape of the cycle-up characteristic leaving the saturation value essentially unchanged. Sample-to-sample variability of the entire characteristic was, however, observed. Maximum variation in saturation residuals achieved in sample films of comparable thickness and preparation conditions, but fabricated from diverse starting material, never exceeded a factor of 5. The maximum observed saturation residual corresponded to less than 10^{14} trapped holes cm^{-3}. Cycle-up for electron residuals was complicated in some samples by hole injection from the substrate. Typically, first-cycle electron residuals were much larger than those for holes reflecting the ratio of respective $\mu\tau$ products for both carriers.

It is important to establish criteria to distinguish when the saturation residual potential is a measure of the integrated density of deep traps. Let N be the density of traps in a specimen. Let n^+ be the number of trapped charges at any time t. $N-n^+$ is the number of unfilled traps at that time. Let ν be the cycling frequency and τ the average release time of a trapped charge (i.e., central release time in the case of a distribution). Then

$$\frac{dn^+}{dt}=K(N-n^+)\nu-\frac{n^+}{\tau} , \tag{7}$$

where $K\equiv$const. At saturation $dn^+/dt=0$ and

$$n_s^+=KN\nu/(1/\tau+K\nu) .$$

There are two limits:

(a) $1/\tau>>K\nu$, therefore

$$n_s^+=KN\nu/(1/\tau)$$

but

$$\tau=\tau_0\exp(E/kT) ,$$

and therefore

$$n_s^+=KN\nu\tau_0\exp(E/kT) . \tag{8}$$

In this limit n_s is linear in the cycling rate and would generally have very strong temperature dependence.

(b) $1/\tau<<K\nu$, and

$$n_s^+=N , \tag{9}$$

the total trap density.

Analysis of cycle-up is most conveniently performed in the electroded xerographic configuration where specimen temperature and cycling rate are easily varied over a wide range. In an amorphous selenium-film contact charged to 200 V five hundred cycles carried out (a) at room temperature with a cycling time of 1 sec and (b) and (c) at 2.4 °C at cycling times of 0.45 sec and 2.65 sec, respectively, were examined. Saturation values of the residual were comparable in all cases despite the factor of 6 variation in cycling rate and the 20 °C temperature change, indicating that the measured space-charge density represents the total trap density.

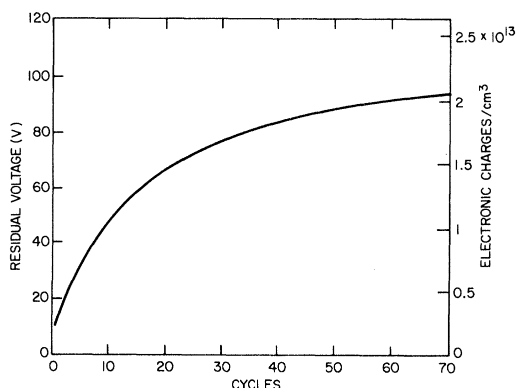

FIG. 3. Positive residual voltage in a 50 μm a-Se sample vs number of cycles. Equivalent bulk density of trapped electronic charge is displayed on the right ordinate scale.

B. Residual decay

When cycling terminates, the residual voltage which has built up begins to decay as the sample undergoes thermally induced relaxation toward space-charge equilibrium. Analysis of the temperature and time dependence of this process maps the spectral distribution of filled traps in the bulk which are now thermally depopulating. It is assumed that charges released from traps are swept out of the bulk, not retrapped. That assumption becomes less valid as the decaying residual voltage

approaches the value of the first-cycle residual. The error introduced in completely neglecting retrapping leads to a slight overestimation of the width of the trap distribution and of the depth of the deepest traps. The analytical procedure follows lines similar to those used in conjunction with other thermally stimulated relaxation processes in solids.[13] Figure 4 compares the respective decays at 298 K of hole and electron residuals in a-Se. Plotted are the log residuals at time t normalized to their initial values V_R^0. It is evident that the electron residual decays much more slowly indicating that in a-Se electrons are more deeply trapped than holes. By varying temperature, parametric sets of decay curves are generated. The latter are illustrated in Fig. 5 for holes and in Fig. 6 for electrons. The procedure adopted here is to represent the decaying voltage as a summation over effective contributions from i trap levels:

$$V(t)=\sum_i C_i \exp\left[-\frac{t}{\tau_i}\right], \quad (10)$$

where the trap release time for the ith trap is

$$\tau_i^{-1}=\nu_i^* \exp(-E_i/kT), \quad (11)$$

and ν_i^* is the attempt to escape prefactor. The voltage is normalized to its initial value V_R^0. Coefficients C_i represent the fractional contribution

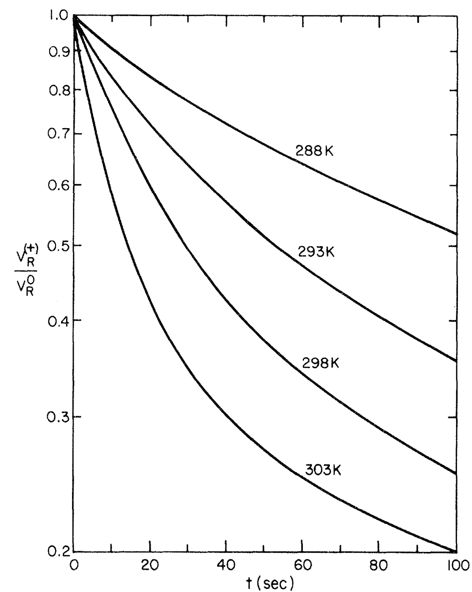

FIG. 5. Parametric set of normalized decay curves for hole residual in $L=50$ μm a-Se film represented in a semilog plot. Temperatures are indicated.

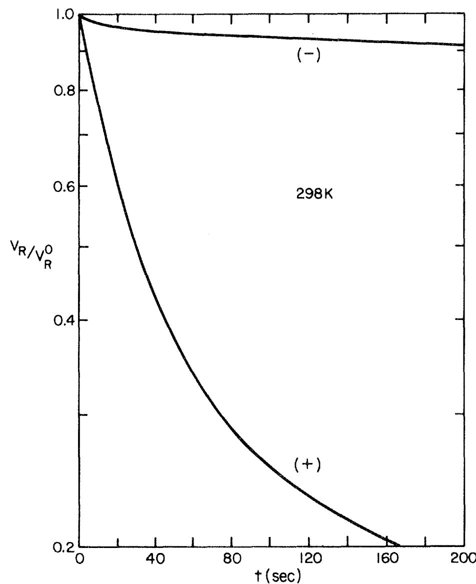

FIG. 4. Semilog plot of decaying electron and hole residuals in a-Se. Residual V_R at a given time is normalized to its value V_R^0 at $t=0$. $T=298$ K, $L\sim 50$ μm.

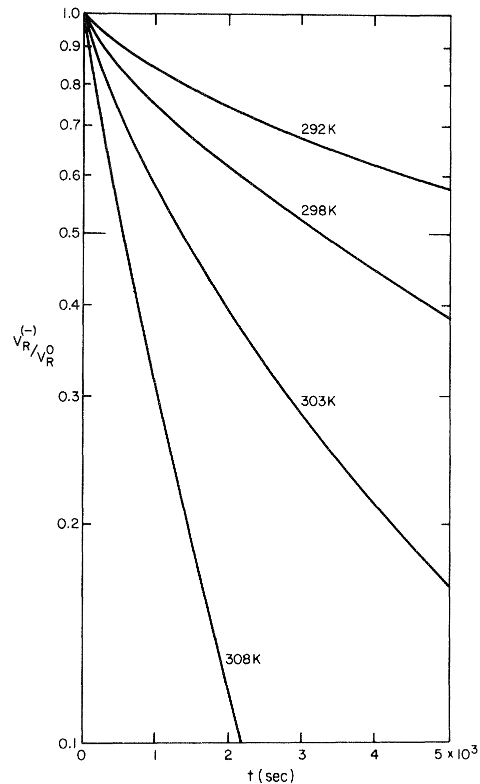

FIG. 6. Parametric set of normalized decay curves for electron residual in $L=50$ μm a-Se film represented in a semilog plot. Temperatures are indicated.

from a level characterized by release time τ_i whose explicit temperature dependence in Eq. (11) defines a trap depth E_i. The set of values C_i, E_i can be used to construct a density-of-states histogram. The above procedure is a particularly appropriate representation of the a-Se data which can be self-consistently fit for both electrons and holes over a range of temperature (i.e., C_1, ν_1^* are temperature independent) with just a few terms in the series represented by Eq. (10). Figure 7 emphasizes an important feature of the data shown in Fig. 5. The log of the initial rate of hole residual decay, representing about 25% of all the charge released from traps during relaxation, is plotted versus reciprocal temperature. The activation energy 0.87 eV represents a fairly discrete low-energy threshold for the deep hole trap distribution which is observed to extend to at least 0.95 eV. The relaxation time τ_{initial} which is 35–40 sec at 298 K is much longer than any limiting instrumental time constant. In the mechanical scanning apparatus, which uses a reciprocating table for instance, the practical time-constant limitation at 298 K would render any state shallower than 0.76 eV invisible.

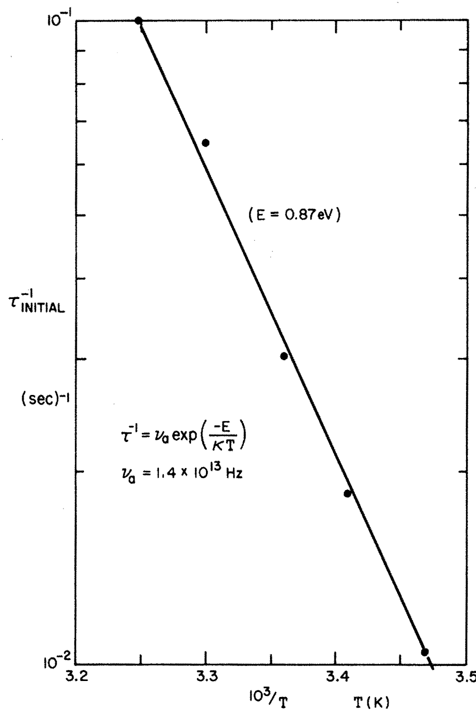

FIG. 7. Semilog plot of initial rate of hole residual decay vs $10^3/T$ in a-Se. Activation energy $E=0.87$ eV represents the low-energy threshold for the distribution of deep hole traps (see text). ν_a is computed from the figure.

In the motionless transient contact-charging apparatus, on the other hand, the limiting time constant is that of the electrostatic voltmeter (or is determined by conditions of illumination) enabling us to resolve the contribution from much shallower states. The ability to vary sample temperature, in any case, significantly diminishes this response-time limitation. If measurements were restricted to a single temperature, for instance, it might be argued that the traps contributing to residual are tail states, that is, they are an experimentally visible component of a distribution extending to much lower energies.[14] If this were the case one would clearly not expect the behavior illustrated in Fig. 7 and would in fact also predict a substantial increase in the saturation residual voltage as the temperature is lowered to unmask more states. The latter is not observed in a-Se. There are two principal features that emerge for the deep gap in a-Se when it is presumed that emerging charges are released to transport states at the mobility edge. A submanifold of states which act as hole traps commences rather abruptly about 0.87 eV from the valence-band mobility edge and extends to a depth about 0.95 eV from the valence-band mobility edge. A second submanifold of states which act as electron traps are peaked about 1 eV from the conduction-band mobility edge and are distributed over a range of about 0.06 eV. The relative position of these features depends on the value assigned to the mobility gap. This value, which must be estimated, is taken to be 2.1 eV, a value just slightly larger than the optical gap.[14] Analysis of thermal generation places the Fermi level in the relative void, near midgap, straddled by these states.

C. Dark decay

In a-Se bulk thermal generation is controlled by localized states which act as hole generation centers. This conclusion is based on observation of the buildup of negative residual space charge as xerographic dark decay proceeds. The buildup of negative space charge can be monitored by the xerographic time-of-flight technique (XTOF). At any time during dark decay a weak flash of strongly absorbed light initiates a small signal hole transit pulse. From the shape of this pulse the nature and distribution of bulk space charge can be determined. It is concluded that negative immobile bulk space charge is generated upon release of free holes from the localized generation centers. Free

holes move to the rear interface neutralizing the resident negative counter charge, in effect transferring that charge to the bulk. The magnitude of the dark decay of the surface voltage can be adequately accounted for on the basis of this negative bulk space-charge buildup. The position of the Fermi level with respect to the valence-band mobility edge is determined to be about 1 eV from analysis of the initial dark-decay rate.[1,15] This estimate is also consistent with the residual decay data which would place the Fermi level further than 0.95 eV from the valence-band mobility edge. The latter value would correspond to the deepest hole traps which are experimentally visible. *a*-Se is thus a *p*-type semiconductor. Use of this value for the Fermi energy and assuming a microscopic mobility of one at room temperature would make the room-temperature conductivity about 10^{-17} $\text{ohm}^{-1}\,\text{cm}^{-1}$.

D. Density-of-states diagram

In Fig. 8 results of residual measurements are combined with information based on analysis of earlier time-of-flight studies[7] (drift mobilities) to construct a composite density-of-states diagram for

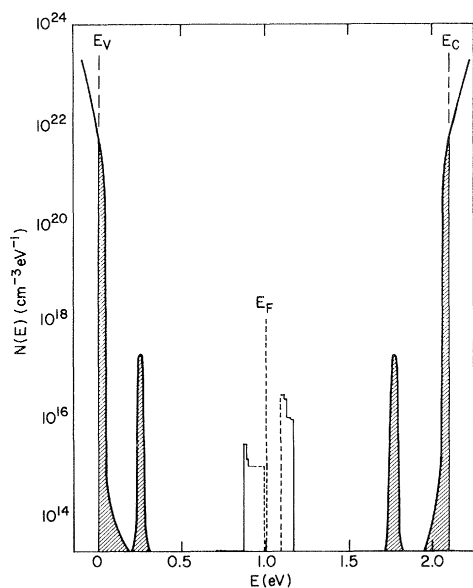

FIG. 8. Composite electronic density of states diagram for *a*-Se. Lobes at 0.25 and 0.33 eV are from analysis of transport data. Remaining structure from analysis of xerographic measurements (see text). Band tails are not measured but are represented schematically.

a-Se. It is assumed that gap states emit their charges to states adjacent to the respective mobility edges.[14] Shallow states which control hole and electron transport form narrow manifolds located 0.25 and 0.33 eV, respectively, from the valence- and conduction-band mobility edges. The deep gap in *a*-Se is characterized by a small, integrated trap population of about 10^{14} cm^{-3}. It is in fact this low density of deep traps in *a*-Se which underlies its utility as a xerographic photoreceptor under cyclic conditions. The very low trap density near midgap is consistent with time-of-flight lifetime data and with earlier, less precise estimates based on trap-limited, space-charge-limited current measurements.[16] Deep trap distributions for both electrons and holes form discrete submanifolds distributed over 0.06–0.10 eV as shown. The voids and relatively sharp demarcation energies for the deep gap-state manifolds are deduced from analysis of the temperature dependence of residual decays. As stated earlier, examination of samples prepared from different source materials display some systematic variability. Samples exhibiting relatively low first-cycle hole residuals are, for example, also those with the narrowest energy distribution of deep-hole traps. Conversely, samples exhibiting particularly high first-cycle hole residuals are those for which the respective hole deep trap distributions are broadest. Broadening of the distribution occurs toward the deep gap leaving the shallow end, characterized by its relatively sharp demarcation energy, unchanged. Despite this degree of variability the impressive feature observed when many *a*-Se samples are examined is, in fact, relative constancy of the deep gap-state distribution.

E. Induced changes in deep trapping

It is possible to effect changes in electron and hole deep trapping in *a*-Se. These changes can be monitored using xerographic techniques. Three mechanisms for inducing change have been identified. They are as follows:

(1) thermostructural,[7,17]
(2) photoinduced, and
(3) chemically induced.[18,19]

(1) and (2) are transient changes which can be induced in any given specimen. In other words, that specimen will subsequently recover its original properties. In (3) *a*-Se films are prepared from chemically modified source material. Changes in electronic behavior relative to undoped material are

permanent. (1) and (2) can be used as tools[6] for probing the origin of naturally occurring deep traps in *a*-Se. The following discussion will deal with the transient-induced effects (1) and (2). Chemical effects are presently under active investigation. The extent to which photoelectronic behavior in any amorphous chalcogenide can in fact be modified by doping (e.g., the degree to which E_F can be unpinned) persists as a major scientific issue.

(1) Structural relaxation is induced in any *a*-Se film by heating it to above T_g and allowing it to anneal there, then quenching it to room temperature. The effect of this procedure is to simultaneously increase both hole and electron deep trapping and this is manifested in both first-cycle and saturation residual potentials. The effect is illustrated in Fig. 9. In Fig. 9 the log of the residual voltages, after ten cycles, $V_R^{(-)}$ for electrons (top curves) and $V_R^{(+)}$ for holes (bottom pair of curves) are displayed as a function of time (note the differing time scales, top for electrons, bottom for the

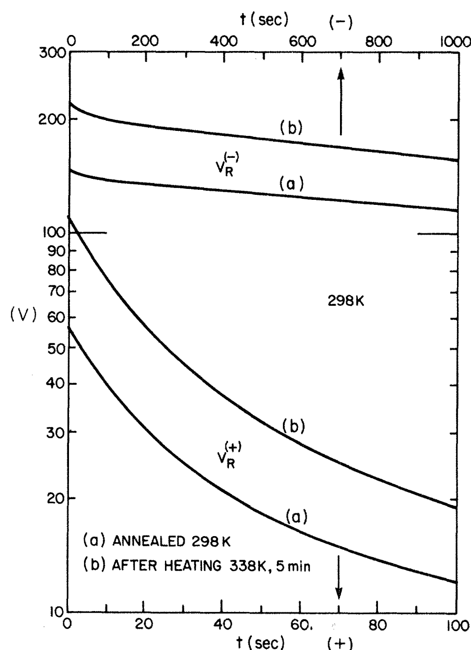

FIG. 9. Semilog plot of decay of electron $V_R^{(-)}$ and hole $V_R^{(+)}$ residual potentials at 298 K. Vertical arrows indicate respective time scales for $V_R^{(-)}$ top and $V_R^{(+)}$ bottom. For each data set ($V_R^{(-)}, V_R^{(+)}$) the lower curve is obtained on a specimen annealed for several hundred hours at room temperature. The curve corresponding to the higher residual potential at 298 K is measured immediately after the specimen has been thermally cycled to 338 K annealed there for 5 min and quenched. Number of cycles fixed at 10.

holes). Curves *a* are for the well-annealed specimen, curves *b* for a twin specimen heated to 338 K for 5 min, then quenched to 298 K. It is clear from the figure that the residual for both electrons and holes is increased immediately after thermal cycling. Complete recovery, $b \rightarrow a$, occurs with room-temperature annealing. The parallel shifts in the curves mean that while the number of trapped charges in the bulk after comparable cycling has increased there is no signficant accompanying shift in the spectral distribution of the traps involved. The excess population of electron and hole deep traps anneal away at the same rate. Xerographic behavior characteristic of the well-annealed film is reproduced after annealing on the order of hundreds of hours at 298 K.

There is a completely analogous effect on xerographic dark decay (thermal generation rate). Relaxation-induced changes in deep trapping have also been observed in trap-limited, space-charge-limited current measurements on *a*-Se.[17] The effect of thermostructurally induced change on deep states in *a*-Se, those that control thermal generation and injected carrier lifetimes, are reminiscent of similar effects reported in earlier studies of transport behavior.[6,7,17] Drift mobilities of electrons and holes in *a*-Se are controlled by localized gap-state submanifolds located a few tenths of an eV from the respective mobility edges as shown in Fig. 8. During relaxation, correlated changes are observed in both electron and hole shallow-trap populations. We suggest therefore that key, localized electronic states (in a given *a*-Se film), though widely distributed throughout the mobility gap, vary in number (though not in spectral distribution) with the structural state of the glass achieving an equilibrium population in the fully relaxed state ($T = T_A$). The correlations between corresponding electron and hole states which can be observed in *a*-Se because of its ambipolarity are nominally consistent with predictions of native defect models[20,21] proposed for chalcogenides. Films prepared from the same source material are observed to have comparable injected carrier lifetimes. Some variability in carrier lifetime is observed when films prepared from different batches are compared.[18] Defect models predict that the latter would result from an interplay between native defects and chemical impurities. This predicted interplay is presently under investigation.

(2) Deep trapping of both injected holes[22] and electrons is temporarily enhanced in an *a*-Se film which has undergone prior photoexcitation with

near band-gap light (600–700 nm). The latter is the excitation region identified with low-temperature photoluminescence, photoinduced electron-spin resonance (ESR), and reversible photostructural effects in a-Se.[23,24] These effects have been interpreted in terms of photoinduced interconversion of native charged defects. It has been proposed that native defects in chalcogenides can interconvert depending on occupancy. That is, they can be empty or contain one charge which makes them neutral or two which reverses their charge sign. It is to be emphasized that metastable deep trapping, in the present case, occurs in the room-temperature range and involves far fewer states than the number presumably implicated in either luminescence behavior, or photo ESR. The decay rate constants for metastable deep trapping (i.e., persistence of the effect) and the time for these metasable traps once filled, to empty (release times), can be distinguished and separately measured by the following xerographic technique. The sample is first exposed to band-edge light for a fixed time generating hole-electron pairs in the bulk. Those that do not recombine eventually fall into deep traps. After illumination has terminted, the sample is dark-rested for a given time τ, which is an experimental variable. At time τ, either electron or hole residual voltage is measured. Residual voltage versus τ values are tabulated and from this data a relaxation function for photoenhanced residual (either sign of space charge) is calculated. Trap release times can be measured in the usual way by monitoring the decay of residual voltage. In the residual voltage measurement (at time τ) the sample is charged and then one sign carrier is injected during surface photoexcitation. It is important to recognize that under these experimental circumstances (i.e., prior to bulk photoexcitation) a residual could arise during charging simply because one sign of bulk-trapped carrier is swept out before xerographic discharge, leaving a net bulk space charge of opposite sign. The appearance of enhanced residual for both signs of charging eliminates this possibility. In addition, there is no evidence of sweep out when the charging current is analyzed. Principal results are the following:

(a) There are distinct decay times (long compared to equilibrium trap release times) for the persistance of metastable hole and electron deep trapping. Metastable electron traps decay away much more slowly than their hole counterparts.

(b) In both the dark-rested and photoexcited sample, at fixed temperature average release time of trapped electrons remains much longer than average release time of trapped holes.

(c) After subband-gap photoexcitation, thermal generation in the bulk is enhanced.

(d) For fixed exposure the photoenhanced trapping effect is about the same for electrons and holes.

A complete discussion of these results will not be presented here; however, at least two general alternative explanations for this behavior are suggested. The first is that photoexcitation by inducing structural change directly creates new gap states which act as traps. The second is that creation of hole-electron pairs in the neighborhood of a preexisting site activates via a trapping event the formation of a recombination center or larger cross-section trap. In fact subband-gap optical quenching of photoconductivity has been reported recently in a-Se.[25] If there is a fixed density of convertible sites then saturation of trap photoactivation should occur with increasing light exposure and this is experimentally indicated. It would be instructive to initiate bulk deep trapping without photoexciting the bulk. Preliminary injection experiments which result in the bulk trapping of only one sign carrier, followed by probe xerographic experiments (like those described above), have recently been initiated.

IV. SUMMARY

Principal results are summarized as follows.

(1) The xerographic process is a sensitive and direct technique for studying deep gap states in wide-band gap amorphous semiconductors. The distribution of deep gap states can be derived from analysis of the buildup during xerographic cycling and the subsequent isothermal decay of surface voltage due to trapped space charge.

(2) A composite picture of the electronic density of states has been deduced from xerographic measurements on a-Se. Gap states form relatively discrete submanifolds, that is, they are separated by regions relatively devoid of states. The integrated number of deep traps is of order 10^{14} cm^{-3} ($E \geq 0.6$ eV). The integrated number of traps, but not their spectral distribution, changes during structural relaxation supporting the view that key gap states are defect derived in chalcogenides.

(3) The distribution of deep traps is, despite their small integrated number, a reproducible property of well-annealed a-Se films. Deep trapping can, however, be affected by thermostructural (relaxation induced) change, subband-gap photoexcitation, and chemical modification (doping).

[1]See R. M. Schaffert, *Electrophotography* (Focal, New York, 1975).

[2]L. B. Schein, Phys. Rev. B 10, 3451 (1974).

[3]A. R. Melnyk, J. Non-Cryst. Solids 35 & 36, 837 (1980).

[4]J. Mort and I. Chen, in *Applied Solid State Science,* edited by R. Wolfe (Academic, New York, 1975), Vol. 5, p. 69.

[5]S. B. Berger, R. C. Enck, M. E. Scharfe, and B. E. Springett, in *The Physics of Selenium and Tellurium,* Vol. 13 of *Springer Series in Solid State Sciences,* edited by E. Gerlach and P. Gosse (Springer, Berlin, 1979).

[6]M. Abkowitz and R. C. Enck, J. Non-Cryst. Solids 35 & 36, 831 (1980).

[7]M. Abkowitz, in *The Physics of Selenium and Tellurium,* Vol. 13 of *Springer Series in Solid State Sciences,* edited by E. Gerlach and P. Gosse (Springer, Berlin, 1979).

[8]M. Scharfe and M. D. Tabak, J. Appl. Phys. 40, 3230 (1969).

[9]See H. Scher, in *Photoconductivity and Related Phenomena,* edited by J. Mort and D. M. Pai (Elsevier, New York, 1976), p. 71.

[10]K. K. Kanazawa and I. P. Batra, J. Appl. Phys. 43, 1845 (1972).

[11]M. D. Tabak and P. J. Warter, Jr., Phys. Rev. 173, 899 (1968).

[12]See F. K. Dolezalek in Ref. 9, p. 27.

[13]D. V. Lang, in *Thermally Stimulated Relaxation in Solids,* Vol. 37 of *Springer Series Topics in Applied Physics,* edited by P. Braunlich (Springer, Berlin, 1979), p. 93.

[14]N. F. Mott and E. A. Davis, *Electron Processes in Non-Crystalline Materials* (Clarendon, Oxford, 1971).

[15]S. W. Ing, Jr. and J. H. Neyhart, J. Appl. Phys. 43, 2670 (1972).

[16]G. Pfister and A. I. Lakatos, Phys. Rev. B 6, 3012 (1972), and references therein.

[17]M. Abkowitz and D. M. Pai, Phys. Rev. B 18, 1741 (1978).

[18]M. D. Tabak and W. J. Hillegas, J. Vac. Sci. Technol. 9, 337 (1971).

[19]J. Schottmiller, M. Tabak, G. Lucovsky, and A. Ward, J. Non-Cryst. Solids 4, 80 (1970).

[20]N. F. Mott, E. A. Davis, and R. A. Street, Philos. Mag. 32, 961 (1975).

[21]M. Kastner, D. Adler, and H. Fritzsche, Phys. Rev. Lett. 37, 1504 (1976).

[22]S. B. Berger, R. C. Enck, and G. M. T. Foley, in *Proceedings of 1980 International Symposium on Industrial Uses of Selenium and Tellurium, Toronto, Canada* (Selenium Tellurium Development Association Inc., Darien, CT, 1980), p. 179.

[23]R. A. Street, Adv. Phys. 25, 397 (1976).

[24]S. G. Bishop, U. Strom, and P. C. Taylor, Phys. Rev. Lett. 34, 1346 (1975).

[25]C. Vautier and C. Viger, in Ref. 7, p. 222.